Determination of residual stress within complex-shaped coarse-grained cobalt-chrome biomedical castings

Brian P. Conroy and David A. Tanner[1]

Department of Design and Manufacturing Technlology & Materials and Surface Science Institute, University of Limerick, Limerick, Ireland

Abstract

ASTM F75 femoral knee implant casting components distort during manufacture due to residual stress re-distribution or inducement. These castings pose a number of challenges for residual stress determination methods; they have a complex geometry, their micro-structure is inhomogeneous, they work-harden rapidly and they have a coarse, elastically-anisotropic grain structure. The contour method is anticipated to be the most promising residual stress determination technique. X-ray diffraction is feasible for components which have experienced plastic deformation on their surface which results in refined diffracting domains. Centre-hole drilling is feasible, but the influence of stress induced from drilling and the effect of coarse grain-structure is unknown. Neutron diffraction is challenging also due to a coarse grain structure and difficult nuclear material properties.

Keywords: Residual stress determination, ASTM F75, CoCrMo, investment casting, femoral knee implants, distortion, coarse grain structure, elastic anisotropy.

[1] Corresponding Author. Email: david.tanner@ul.ie

1 Introduction

Femoral knee implants, referred to as "femorals" in this article, are one component of a total-knee-replacement which restores functioning articulation to the patient. It is estimated that 720,000 knee replacement procedures were carried out in 2014 in the US alone[1, 2] with this figure predicted to grow to 3.48 million by 2030 (Ref. [3]). ASTM F75, a Cobalt-Chrome-Molybdenum (Co-Cr-Mo) material, is favoured for load bearing, moving-contact applications, such as required for knee implants, due to excellent wear, corrosion and bio-compatibility properties[4-6]. The typical manufacturing route for femorals is investment casting[7] and subsequent machining processes.

As a result of the required articulation and in-service performance criteria, femorals are complex shaped components[8] whose dimensions vary greatly as a large range of products and sizes exist. A typical femoral has a varying thickness of 2 – 8 mm (see Figure 1) and the entire component could fit within a 70 mm cube. The basic shape of a femoral can be described as a "*C*" [8] (see Figure 1 and Figure 2). The dimension across the open end of the "C", the Anterior-Posterior (A-P) dimension, can vary following material removal processes. This dimension is considered critical in order to ensure optimum fit to the patient's bone and therefore parts which fall out of specification are rejected resulting in significant environmental and business costs.

Residual stress is the source of this part distortion, as will be outlined in section 2, with a number of other factors, such as elastic-anisotropy, potentially influencing the magnitude of this distortion. In order to investigate the effect of various manufacturing processes on the parts' residual stress, a reliable determination method is required. However, currently no literature exists on the application of residual stress determination methods to cast ASTM F75 implants.

As outlined in Ref. 9, the selection of a suitable residual stress determination technique requires careful consideration of the component, the location and gradient of the stress of interest. In addition to these considerations are the technical requirements and limitations of each technique, many of which are material and geometry dependent.

The objectives of this paper are to:

- Determine the origins of residual stress for cobalt alloys.
- Define the mechanisms of part distortion during the production of ASTM F75 femorals.
- Review residual stress determination methods for application to complex geometries with a specific focus on femoral castings.
- Review residual stress determination methods for application to coarse and elastically anisotropic grain structures.
- Review residual stress determination methods for application to materials which rapidly work-harden.

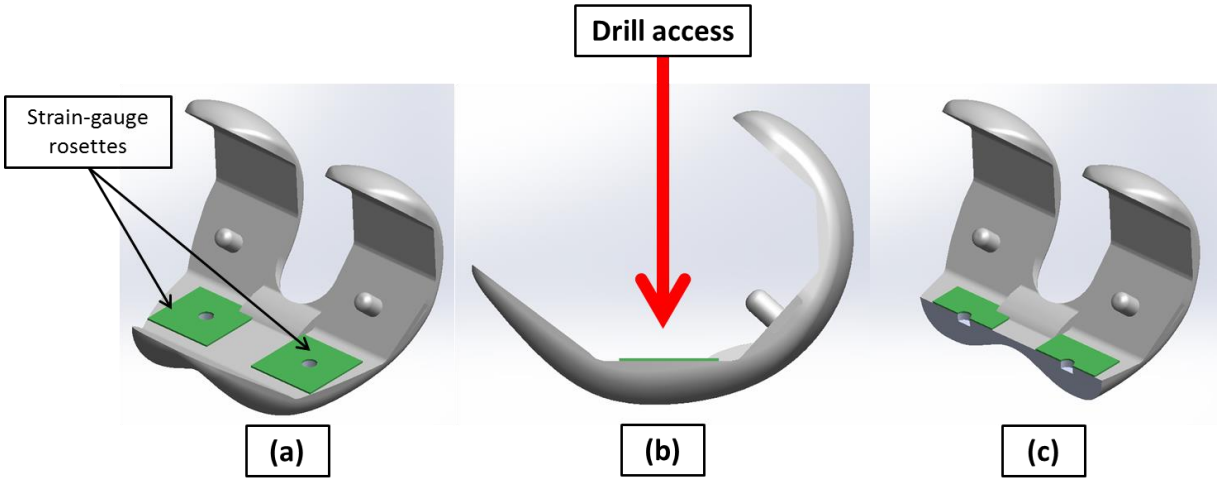

Figure 1. CAD representation of the femoral component. Detail of the centre-hole drilling set-up is also shown and will be outlined in section 4.2.3.1. Image (a) shows the two possible locations for application of the centre-hole drilling method. Image (b) shows drill access limitations. Image (c) is a cross-section through the drilled holes, the varying femoral thickness can be observed.

2 Implant distortion

Residual stress is defined as stress remaining in a component in the absence of external loading[10-13], the origins of which are well reviewed[11-16]. Residual stress is the elastic response to incompatible strains[16] which are the result of inhomogeneous shape misfits, for example due to non-uniform plastic deformation or phase transformation[14]. The following are hypothesised as possible means of inducing residual stress in ASTM F75 femorals during production:

- Non-uniform plastic flow as a result of mechanical deformation and/or thermal gradients.
- Non-uniform volume changes as a result of strain induced Face-Centred-Cubic (FCC) to Hexagonal-Close-Packed (HCP) martensitic phase transformation[15, 17-21].

ASTM F75 is a difficult material to machine (see section 3.3), therefore complex shaped components, such as femorals, are typically investment cast to a near net shape. Following casting a number of manufacturing processes typically exist which have the potential to induce residual stress, including: mould removal, casting cut-off, casting-gate removal, heat-treatments and blasting[7]. Following these potential manufacturing processes the articulating surfaces of femorals are machine ground and polished to achieve high surface finish requirements[8].

With reference to Figure 2 a & b, stress which acts in the hoop direction would be the most influential on the A-P dimension. As material is only removed from the articulating surface, one, or a combination of, the following two occurrences is the cause of distortion (see Figure 2):

- Partial/total removal of a compressive layer of residual stress near the articulating surface.
- The material removal process induces tensile residual stress on the articulating surface.

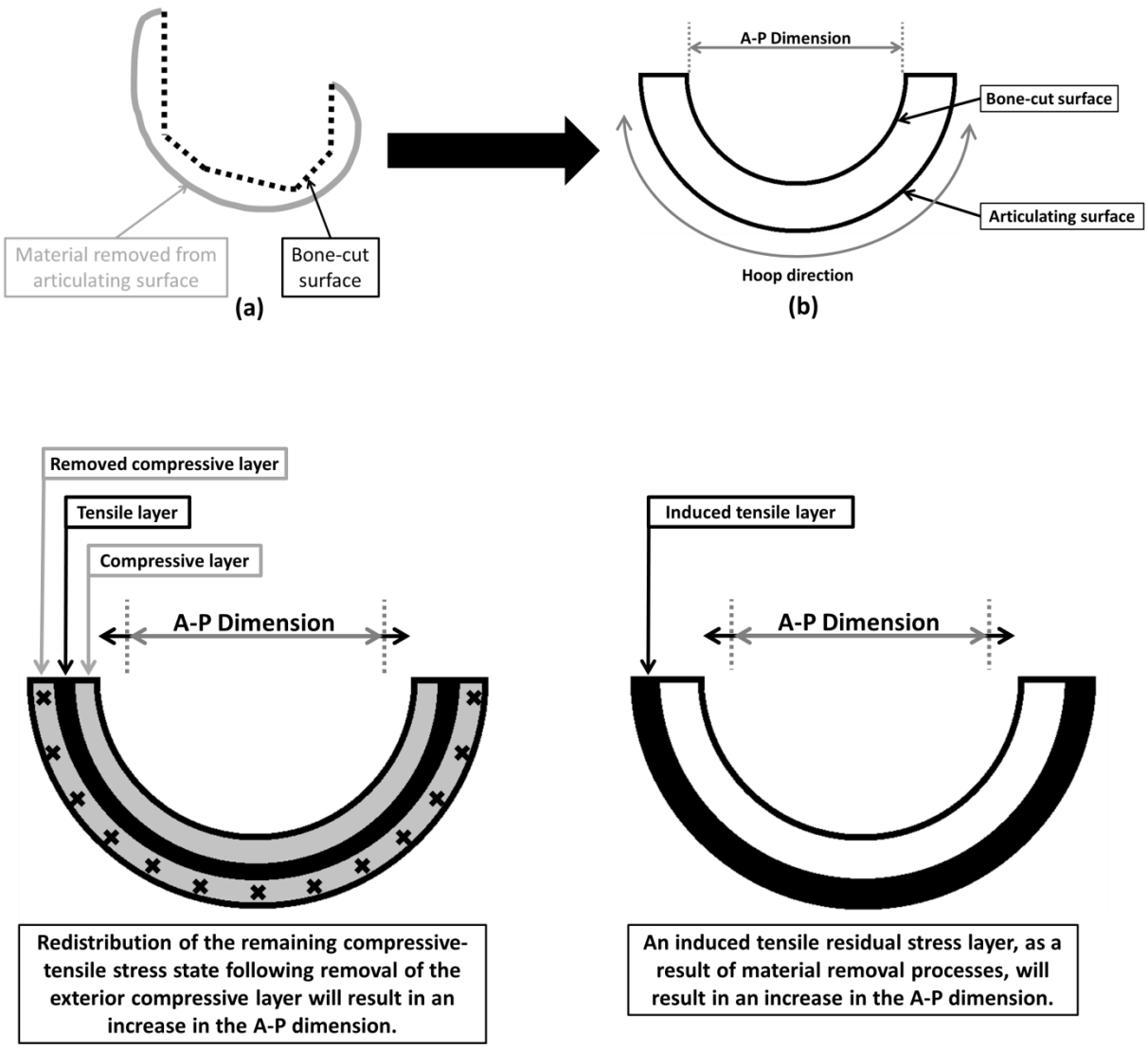

Figure 2. (a) Pictorial cross-sectional view of femoral indicating its main features. (b) Simplification of the femoral as a "C"-shaped component. (c) Description of two possible residual stress related distortion mechanisms.

3 Component characterisation

3.1 Microstructure

3.1.1 Cast ASTM F75

As-cast ASTM F75 has a metastable cobalt-based dendritic FCC matrix at room temperature interspersed with a carbide secondary phase of $M_{23}C_6$ (M = CR or Mo)[17, 20, 22-30]. Some manufacturers apply homogenising heat-treatments in order to eliminate porosity and to improve mechanical properties[22, 29-31]. The following microstructural features can be affected by casting conditions and variations in the initial billet composition[22-24, 29, 31, 32]:

- Morphology, size and area-fraction of the $M_{23}C_6$ carbide phase.
- Dendrite arm spacing.
- Porosity.
- Grain-size.

Given the various different femoral sizes, designs and the cast microstructural features described, the as-cast microstructure can vary significantly.

3.1.2 Grain-size

As-cast ASTM F75 components have large and varied grain-sizes[22, 29, 33-35] that are heavily dependent on cooling-rates influenced by factors including casting-size, mould temperatures and pouring temperatures[22, 33, 35]. In an effort to achieve a more refined grain structure to mitigate the potential of elastic anisotropy (see section 4.2.1), ASTM F75 samples were cast utilising a cobalt alumina inoculant in the prime coat of the investment casting shell[36 37]. The use of inoculants for the production of implants varies depending on the product type and manufacturer. Microstructural evaluation conducted on a femoral which was cast with an inoculant as part of this study (Figure 3), revealed a heterogeneous grain-size due to grain-growth commencing at nucleation sites of the inoculant at the shell wall. Grain-size was still found to be large towards the interior of the casting with diameters of the order of hundreds of micrometres.

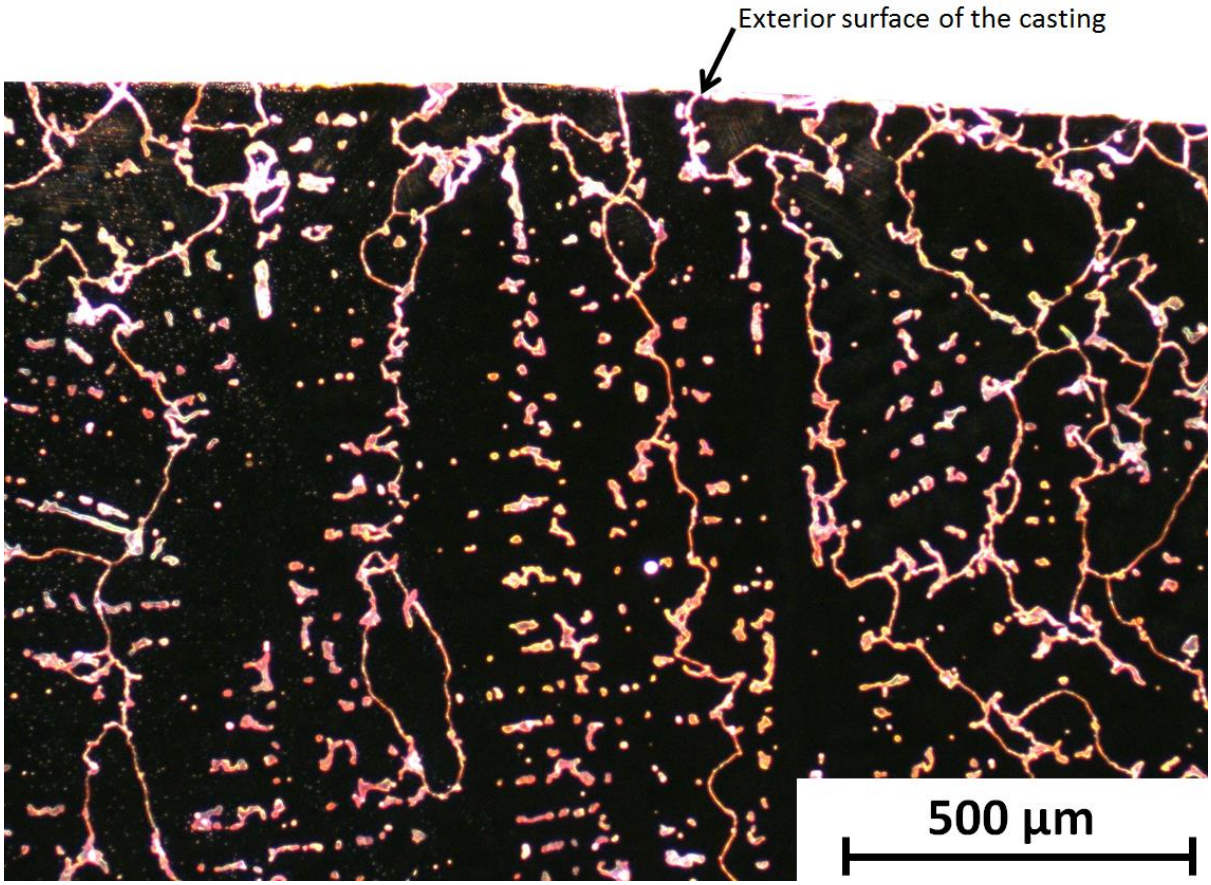

Figure 3. Dark-field optical micrograph of the as-cast structure of an ASTM F75 femoral cast with an inoculant. Electrolytic etching process used: 10% ammonium persulphate solution, 8V DC, negative terminal of cable utilised as the cathode, sample to be etched was the anode. The cathode swiped above the sample surface until a yellow tint was observed (typically 3-5 seconds).

3.2 Elastic modulus anisotropy

Existing literature, outlined in this section, shows that ASTM F75 is strongly elastically anisotropic on the basis of single-crystals or coarse-grained poly-crystalline samples. Additionally, for FCC materials the <100> lattice directions, those with the lowest elastic modulus[38], align with the solidification direction during casting[38, 39, 42]. Two patents[39, 40] exploit this potential to produce implants with controlled elastic modulus as a means to optimise stress distribution from an implant to the patient's bone[39-41]. With ref. [39] stating that it is possible to reduce the elastic modulus of an ASTM F75 casting by 40% in a particular direction by growing a single-crystal. Additionally, the elastic moduli of polycrystalline ASTM F75 tensile specimens were found to vary by ~25% (Ref. [24]). These tensile samples were obtained from cylindrical castings cooled at different rates, which would have influenced grain size and orientation.

The degree of anisotropy and the elastic response of a particular *hkl* direction could be determined should single crystal elastic constants be available[42, 43]. However, single crystal elastic constants specific to ASTM F75 are not currently available in literature, but they do exist for pure cobalt, the elastic anisotropy factor of which was found to be 2.83 (Ref. [42, 44]).

Given that ASTM F75 is highly elastically anisotropic on a single crystal basis and considering elastic anisotropy is evident in poly crystalline tensile samples. It is probable that the coarse-grained femoral castings are elastically anisotropic on a macroscopic scale. The directional elastic properties of the femoral would be dictated by the grain orientations, which are dependent on the solidification direction.

3.3 Work-hardening

ASTM F75 rapidly work-hardens, as can be observed in Figure 4 where ASTM F75 is compared to SAE 430F. SAE 430 F is a free-machining stainless-steel with good machinability characteristics typically used for aircraft fasteners, gears and shafts[45]. ASTM F75's rapid work-hardening is attributed to stacking fault intersections, stacking-fault twins and a strain-induced martensite phase transformation (Ref. [20, 46]). It is this rapid work hardening in conjunction with the materials high ultimate tensile strength (approx. 750 MPa [24]) and high hardness properties (310-350 H_v for the matrix material and as high as 600 H_v for carbides[24]), which makes ASTM F75 a difficult material to machine using conventional methods.

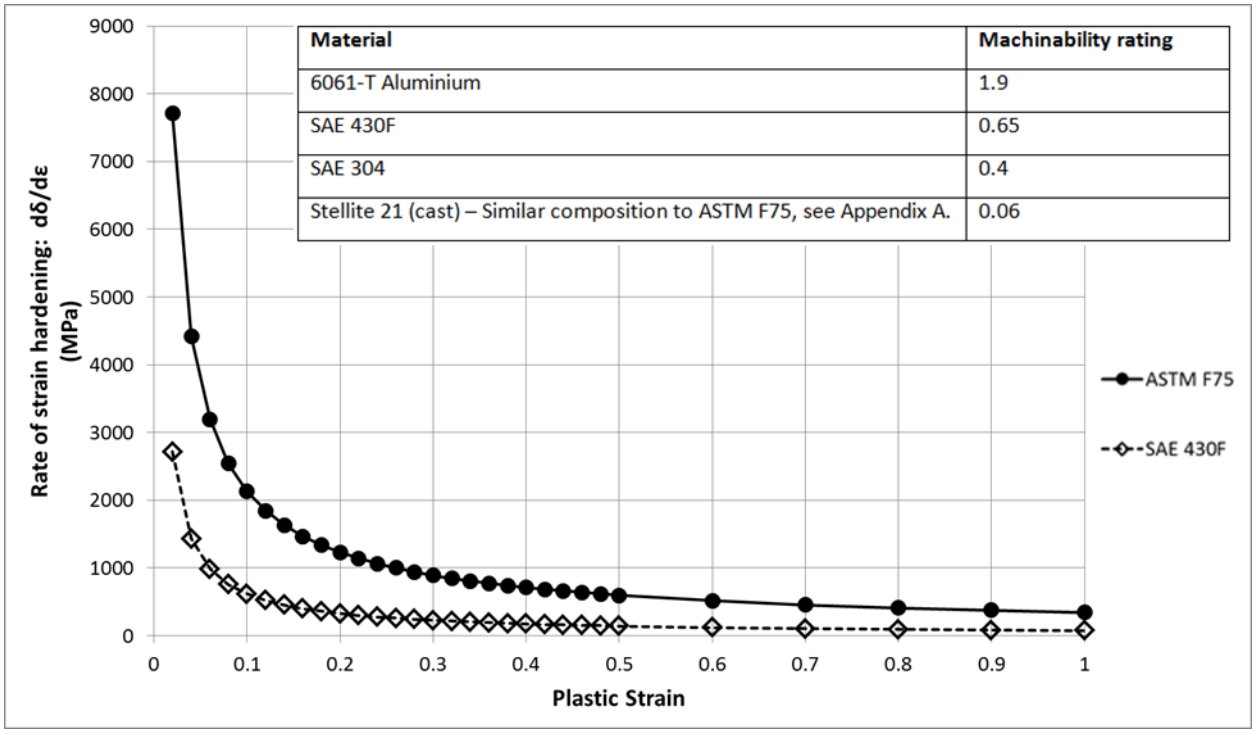

Figure 4 Rate of work-hardening as a function of plastic strain for ASTM F75 and SAE 430F calculated from flow stress data at 25°C and at a strain rate of 1.0. Flow stress data was calculated by JMatPro©[47] software and the rate of strain hardening was calculated from: $\frac{d\sigma}{d\varepsilon} = n\frac{\delta}{\varepsilon}$ *where n is the strain hardening exponent[43]. Machinability ratings shown are relative to that of AISI B1112 steel which is assigned a machinability rating of 1 (Ref. [48]).*

4 Residual stress

4.1 Length scales

Residual stress is classified according to the scale over which it equilibrates[10-13] (see Figure 5):

Type I (Macro residual stress): Residual stress that equilibrates over length scales much larger than the specimen's grain-size.

Type II (Inter-granular stress): Residual stress that equilibrates over length scales of a small number of grains. Type II stress can arise from differing elastic properties between grains or due to misfits between phases in the material[10].

Type III (Micro residual stress): Residual stress that equilibrates within a single grain, i.e. atomic length scales. Type III stress is the result of atomic-scale dislocations and point defects[16].

Distortion of femorals occurs across their entire width and it is therefore Type I residual stress which is of interest. As outlined in section 3.1.2, the grain-size of ASTM F75 castings approach the macroscopic scale, therefore mechanisms of Type II stress could contribute to macroscopic deformation. Type III stress is expected to average to zero over macroscopic gauge volumes.

In a gauge volume of a residual stress determination method applied to a material with more than one phase, Type II and III stress may average to zero. However, phase dependent Type II and III stress may not. Therefore macroscopic stress results obtained using diffraction techniques (see section 4.2.2) which only measure one phase may experience a contribution from Type II and III stress[10].

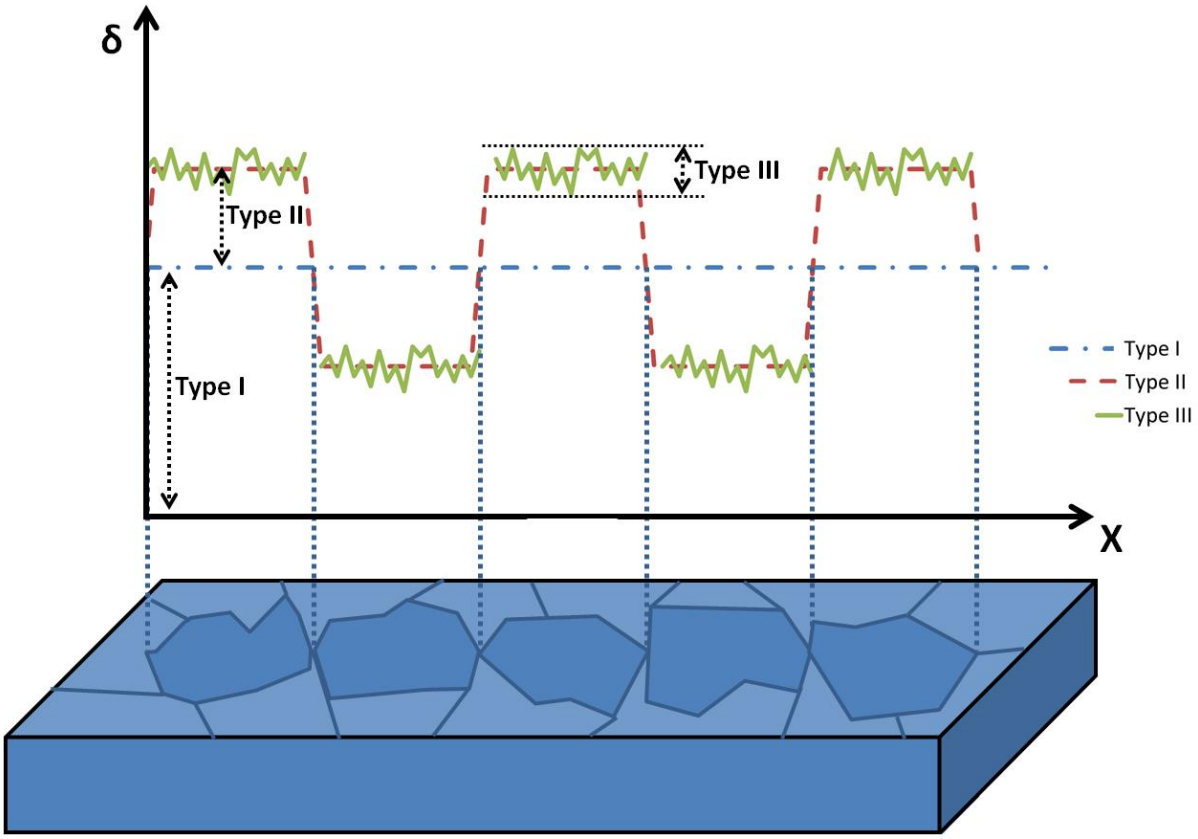

Figure 5. Graphical representation of residual stress length scales (Reproduced from Ref. 11).

4.2 Residual stress determination methods

Residual stress determination methods have been significantly reviewed in existing literature[10, 11, 13, 14, 49-51]. The limitations of a number of techniques for application to ASTM F75 cast femorals are outlined in section 4.2.1 and the feasibility of the following methods are thoroughly reviewed:

- Diffraction techniques (section 4.2.2):
  - X-Ray
  - Neutron
- Strain-release techniques (section 4.2.3):
  - Centre-hole drilling
  - Contour method

4.2.1 Limitations

A number of residual stress determination methods are considered unsuitable for application to cast ASTM F75 implants:

- Layer removal[52] and sectioning[53, 54] methods require geometric symmetry which is not available (see Section 1).
- Magnetic and ultrasonic methods require a homogenous microstructure[10, 11, 13, 55, 56] (see section 3.1.1).
- The ring coring method's[57, 58] gauge volume is too coarse with respect to the femoral geometry outlined in section 1. This method requires a minimum core diameter of *15 mm* to accommodate a *12 mm* diameter strain gauge rosette[59, 60].
- The slitting method[61], for which compliance functions can be determined for complex geometries[62], is not suitable as the spatial resolution of the technique is too coarse.
- The deep-hole drilling method[63] it not suitable as stress-relaxation associated with drilling the initial pilot hole means that results obtained from the initial *~1 mm* depth are uncertain[64].

Residual stress determination methods measure strain from which stress is calculated utilising a variation of Hooke's Law:

$$E = \frac{\sigma}{\varepsilon} \qquad (1)$$

Where; E – elastic modulus
σ – stress
ε – strain

Stress determination methods assume that the specimen has an isotropic elastic modulus, which holds true in the case of materials with fine, equi-axed and randomly orientated grain structures[14, 42]. However, the combination of large grain-sizes (see section 3.1.2) and anisotropic elastic modulus of individual grains (see section 3.2) mean it is possible that gauge volumes of certain residual stress determination techniques could have a directionally dependent elastic modulus.

A number of residual stress determination methods, such as centre-hole drilling, ring coring, deep-hole drilling and X-ray diffraction, require flat surfaces and are therefore not suitable for application to the articulating surface of the femoral[65-67], which is an area of interest. However measurements on the flat bone-cut-surface could still help to determine the influence of various manufacturing processes on bulk residual stress magnitudes.

4.2.2 Diffraction techniques

Diffraction techniques non-destructively determine strain by the measurement of a change in interatomic lattice plane spacing, *d*, between a strained and an un-strained sample[68]. When a beam (x-ray or neutron) of known wavelength, λ, interacts with a crystalline material at the Bragg angle, θ, constructive interference in the diffracted beam occurs, which is identified using x-ray or neutron detectors. Once θ has been determined the interatomic spacing can be calculated using Bragg's law[68]:

$$n\lambda = 2dsin(\theta) \qquad (2)$$

Where; n – order of interference (an integer value)
λ – wavelength
d – inter-atomic spacing
θ – Bragg angle

4.2.2.1 Diffraction elastic constants

Diffraction techniques which utilise a monochromatic wavelength determine strains for one particular crystallographic *hkl* plane. Lattice strain for each *hkl* plane, below an elastic limit, is proportional to the macroscopically applied stress. However, each plane responds differently. Therefore, elastic constants specific to the measured *hkl* plane are required[10]. Diffraction elastic constants are determined by known uniaxial loading of a sample during diffraction experimentation[38, 69].

For both X-ray and neutron diffraction the *{311}* plane is the most suitable for experimentation due to its low sensitivity to inter-granular strain[70] and its high multiplicity factor of *24* (Ref. [71]). Also a benefit for X-ray diffraction is that the *2*θ angle will occur in the region of *153-159°* (Ref. [71]), which ensures reduced calculation errors[71, 72]. Most laboratory-based powder X-ray diffractometers do not have such *2*θ angle capabilities; a residual-stress-specific diffractometer is required.

ASTM F75 elastic constants have not been identified from literature; therefore elastic constants for pure cobalt and a CoCr20Mo10 alloy are reported (see Table 1). At Time of Flight (ToF) neutron diffraction facilities, a diffraction spectrum containing reflections from a number of *hkl* planes is obtained and the use of full pattern analysis returns the lattice parameter. Therefore macroscopic elastic modulus and Poisson's ratio can be utilised, provided the sample is not textured[70].

Table 1. {311} plane elastic constants for Co and a Co-based alloy.

Material	$E_{311}(GPa)$	ν_{311}	**Source**
Pure Cobalt	155	0.36	Calculated utilising the Hills model with single crystal elastic properties[38, 44, 69, 73].
CoCr20Mo10 (similar composition to ASTM F75, see Appendix A)	193	0.33	Ref. [74]

4.2.2.2 X-ray diffraction

The X-ray diffraction residual stress determination method is standardised[71] and a number of useful texts exist[67, 68, 72, 75, 76]. The method allows for non-destructive strain evaluation within a thin surface layer of a crystalline material, approximately *5 μm* deep for cobalt alloys[71]. The method can be combined with layer removal by electro polishing to determine a stress-depth profile[71].

4.2.2.2.1 Material grain-size

Problems with uncertainty in peak location can occur for both excessively small and large-sized grains[71, 75]. Inspection of the entire DeBye ring, i.e. a plan view of the diffraction cone, is required in order to evaluate whether a sufficient number of grains are contributing to X-ray diffraction peaks. "Spotty" Debye rings suggest that the specimen grain-size is too coarse for accurate measurement[72]. Ref. [67] states that rocking a sample during irradiation allows residual stress determination on samples with average grains diameters up to *254 μm* (Ref. [77]).

4.2.2.2.2 Feasibility study

To evaluate the feasibility of X-ray diffraction with cast ASTM F75 femorals, five samples were selected, each with a different processing history, as outlined in Table 2. All samples selected were cast with an inoculant (see section 3.1.2). The samples were irradiated in two orthogonal directions at each point using two different X-ray methods:

- The $sin^2\psi$ method[71, 72] carried out by the University of Manchester (UoM) utilising a Proto X-ray diffractometer.
- The *cosα* (ref. [78, 79]) method carried out by Pulstec Industrial Co. Ltd. utilising their μ-X360 diffractometer.

Both X-ray diffraction methods utilised the *{311}* plane and a manganese X-ray tube[71] in order to avoid fluorescence[51, 71, 72]. Both techniques utilised a *2 mm* diameter aperture, with one exception. For measurement XRD 1, UoM applied a *1.5 mm x 5 mm* aperture in conjunction with a random-pattern oscillation extending 3 *mm* in two orthogonal directions parallel to the samples surface. This was intended to increase the number of diffracting grains within the gauge volume.

4.2.2.2.3 Results and Discussion

X-ray diffraction results are summarised in Table 2. Measurements XRD 1 and XRD 4 did not return useable diffraction spectrums due to a coarse grain structure, which was observed from inspection of Debye rings obtained utilising the Pulstec μ-X360 diffractometer. The manufacturing processes applied to samples utilised for measurements XRD 2, 3 and 5, fractured crystal domains near the surface, resulting in a sufficiently refined grain-size.

Phase dependent microstress may influence X-ray diffraction results, as outlined in section 4.1. Ref [80] outlines three methods for the separation of macro and microstress. Here one method was applied, which was the inspection of the linearity of d vs $sin^2\psi$ plots obtained by UoM for successful measurements XRD 2 and XRD 3. All plots were linear and had no evidence of splitting, which is typical of a uniaxial/biaxial stress state with no texturing effects[72].

Figure 6 shows the sample used for measurements XRD 1 and XRD 5 with the solidification direction indicated. Grain-size is refined in areas of faster cooling[22], as evidenced by the comparison of the number of spots in Debye rings (a) and (c) shown in Figure 6. Measurement XRD 5, made in the area highlighted in black in Figure 6, was on a surface cut by an abrasive wheel. Plastic deformation from the cutting process fractured grains near the surface resulting in a sufficient number of diffraction domains as evident by the continuous Debye ring (b) shown in Figure 6.

As the successful x-ray diffraction measurements exhibited a refined grain structure and considering that diffraction-plane-specific elastic constants were utilised (see section 4.2.2.1), the successful x-ray diffraction results cannot be influenced by the elastic anisotropy concerns highlighted in section 3.2.

It can be concluded that X-ray diffraction is a suitable technique to investigate residual stress arising from manufacturing processes which plastically deform the surface of cast ASTM F75 components. Layer removal may be used to obtain stress-depth profiles, however the potential depths at which residual stress could be determined will depend on the depth over which plastic deformation has fractured crystal domains to a suitable size. The X-ray diffraction technique is not suitable for as-cast or heat-treated ASTM F75 components due

to their coarse grain structure, even with the application of oscillation techniques and the use of inoculants.

Table 2. X-ray diffraction results for ASTM F75 samples with various processing history. All samples were initially cast using an inoculant. X-ray elastic constants utilised: $E_{311} = 193GPa$; $\nu_{311} = 0.33$ (Ref. [74]).

Meas. #	**Sample process history**	***sin²ψ* method (MPa) (UoM)**		***cosα* method (MPa) (Pulstec)**	
		Direction 1	**Direction 2**	**Direction 1**	**Direction 2**
XRD 1	As-cast surface	No peak	No peak	No peak	No peak
XRD 2	Plastically deformed surface[†]	-614 +/- 8	-648 +/- 14	-564 +/- 42	-517 +/- 36
XRD 3	Plastically deformed surface[†]	-729 +/- 26	-698 +/- 22	-809 +/- 59	-894 +/- 49
XRD 4	Heat-treated following surface induced plastic deformation[†]	No peak	No peak	No peak	No peak
XRD 5	Surface cut by an abrasive cutting wheel	Not attempted	Not attempted	1126 +/- 31	Not Attempted

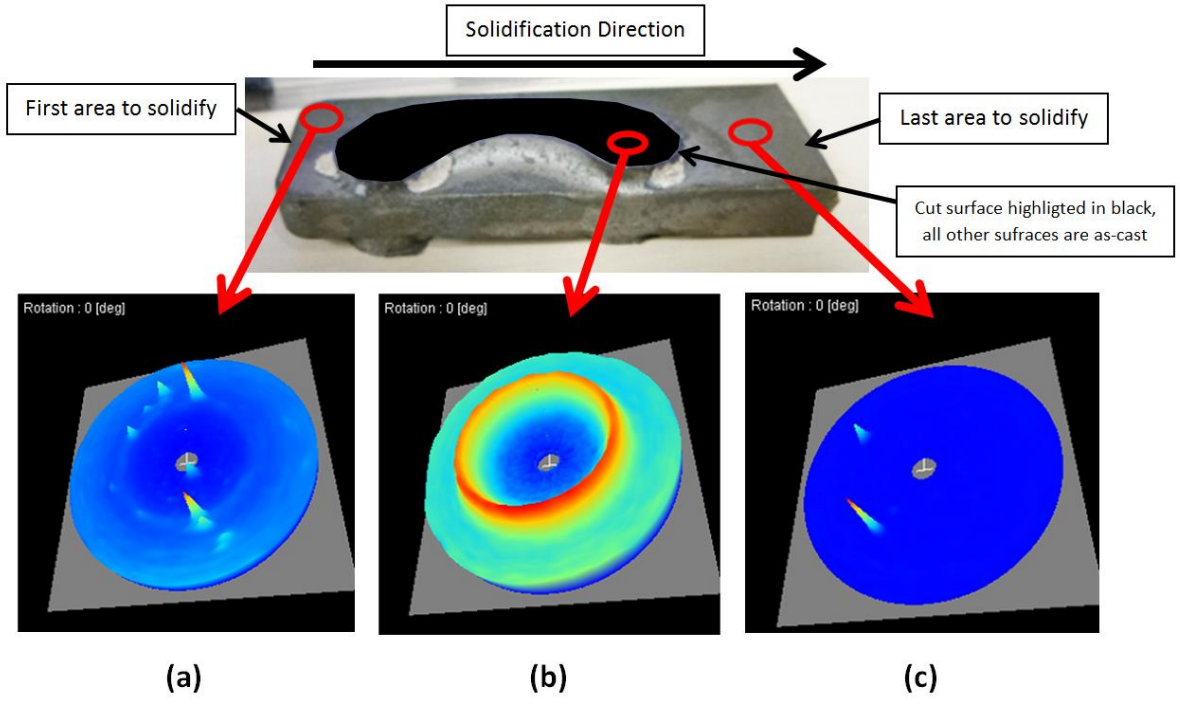

Figure 6. Sample utilised for measurement XRD 1 and XRD 5, inset images (a), (b) and (c) show Debye rings obtained using the Pulstec μ-X360 diffractometer (note, diffraction intensity is represented by the height of the DeBye ring peaks shown). Image (a) and Image

[†] Specific details of manufacturing process cannot be published due to intellectual property restrictions.

(c): Debye rings from measurements XRD 1, note the surface is in the as-cast condition. Image (b): a Debye ring from measurement XRD 5, note the surface, highlighted in black, was cut using an abrasive cutting wheel.

4.2.2.3 Neutron diffraction

Uncharged neutrons have greater penetration ability than X-rays, therefore stress can be determined within the bulk of the material[81]. Neutron diffraction residual stress determination is standardised[70] and a number of excellent guidance publications exist[38, 81, 82].

Depending on the facility, monochromatic or polychromatic wavelengths are available for experimentation. Monochromatic wavelength beams are utilised in a similar fashion to laboratory based X-ray diffraction in that the 2θ location of a single diffraction peak is of interest. Polychromatic neutron beams use the ToF method where the 2θ diffraction angle remains constant and varying wavelengths are used to obtain a diffraction spectrum with reflections from a number of *hkl* planes.

The application of neutron diffraction to coarse-grained, complex-shaped, cobalt alloys is challenging and requires a significant amount of beam-time, as outlined in sections 4.2.2.3.1 and 4.2.2.3.2. To date the authors have conducted two feasibility experiments on cast ASTM F75 specimens:

- ToF applied to a femoral casting using Engin-X at the ISIS Pulsed Neutron and Muon Source, Science and Technology Facilities Council, Rutherford Appleton Laboratory, Harwell Oxford, Didcot, OX11 0QX, UK.
- Monochromatic-wavelength neutrons applied to a “stress-lattice” specimen (see Figure 7) using E3 at the Helmholtz-Zentrum-Berlin, Hahn-Meitner-Platz 1, 14109 Berlin, Germany.

Some initial findings from experimentation are reported here. More detailed publications for each experiment are planned.

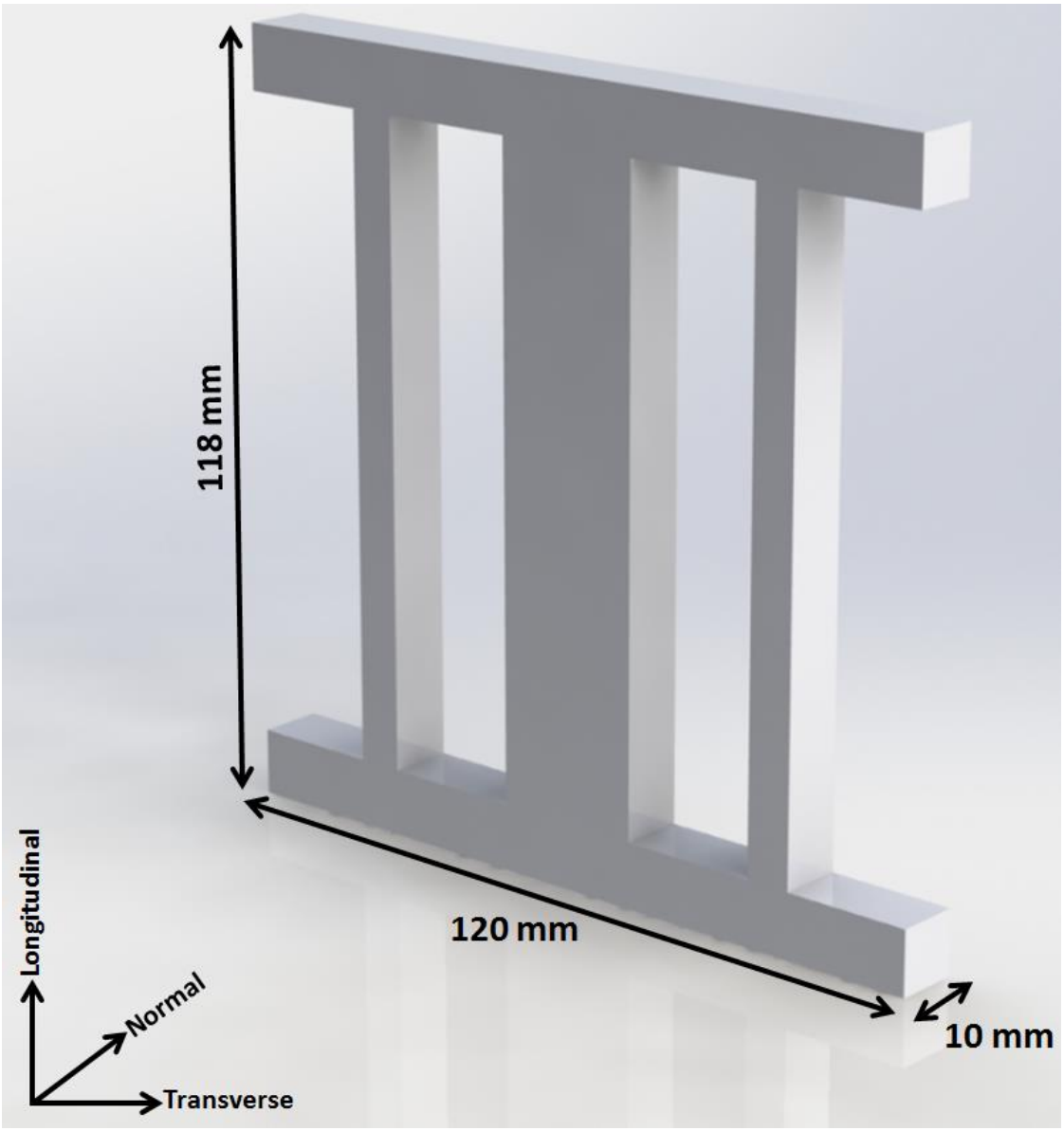

Figure 7. CAD representation of the cast stress-lattice specimen utilised for experimentation on E3 at Helmholtz-Zentrum-Berlin.

4.2.2.3.1 Sample grain-size

Ref. [82] outlines that grain-size effects are noticeable for grains larger than 100 µm, so the samples used in this study were cast with an inoculant. Unfortunately, coarse-grain-sizes still remain within interior regions (see section 3.1.2).

In the case of a coarse-grained material, the number of grains contributing to the diffraction spectrum may not be homogenously distributed throughout the Sample Gauge Volume (SGV), causing a shift in its centroid from that of the Instrument Gauge Volume (IGV). Such a shift, if uncorrected, results in an apparent strain[38 70, 82 83]. Also, as a result of the SGV

centroid shift, the position of strain measurement can change for each strain-vector measurement[38]. An additional concern is the possibility of neutron beam extinction which occurs when a large-grain diffracts out a large-portion of intensity of a particular wavelength, therefore modifying the wavelength composition of the beam which proceeds to subsequent crystals. Extinction can lead to an apparent shift in the diffraction peak[38].

In order to alleviate the effect of coarse grain structure, the number of grains contributing to the diffraction spectrum needs to be increased[83]. This can be achieved by a number of methods:

- Increasing the gauge volume size[83]. Success of this method will depend on the distribution of the diffracting grains within the larger gauge volume[82]. This method can conflict with resolution requirements.
- Rotation of the specimen about an axis perpendicular to the diffraction plane which effectively increases the number of grains from the same gauge volume[82, 83].
- Averaging two neutron diffraction measurements at the same location but at 180^o to each other in order to reduce systematic errors[84].

ToF has a desirable advantage over monochromatic methods in that a diffraction spectrum is obtained over a large 2θ range. Therefore, each grain within the gauge volume should contribute to at least one peak on the diffraction spectrum. Additionally, there would be an angular spread in data collection in the horizontal and vertical planes[82]. However, it was noted from experimentation at Engin-X that peaks were missing from some diffraction spectrums obtained, which suggests an excessively coarse grain structure was present.

4.2.2.3.2 Nuclear material properties of the sample

From Table 3 It can be observed that the incoherent cross-section and absorption cross-section of ASTM F75 is quite large in comparison to Iron and its coherent cross-section is considerably less. It is therefore be expected that ASTM F75 samples would result in long count times, high background noise and measurement path lengths would be limited[85]. Such difficulties were experienced at Engin-X where count times in the region of *2.5 hours* per measurement were required in order to obtain fitting uncertainty in the region of $70\ \mu\varepsilon$ for a *2x2x2 mm* gauge volume with path lengths of *4–10 mm*. Similar measurements for Fe

would take *1.5 minutes*[86]. It was also noted that convergence of peak-fitting analysis of diffraction spectrums from Engin-X was problematic for path lengths beyond *5 mm*.

Count times at E3 varied from *60-160 minutes* per measurement, which obtained average fitting uncertainty ranging from *65 με* (for the normal direction, see Figure 7, where path lengths were *3-10 mm*) to *225 με* (for the longitudinal direction, see Figure 7, where path lengths were *14.2 mm*). At E3, a long "match-stick" type gauge volume, *20x2x2 mm*, was utilised as the stress gradient along the lattices "Longitudinal" direction was not expected to vary significantly (see Figure 7).

It should be noted that uncertainty values for experimentation at Engin-X and E3 are also likely to be heavily influenced by the coarse grain structure of the samples outlined in section 4.2.2.3.1.

Additional difficulties associated with large absorption cross-sections include weak diffraction signals and shifts in the SGV centroid[70] (see section 4.2.2.3.1). Ref. [38] recommends that the maximum dimension of the Nominal Gauge Volume (NGV) be smaller than the attenuation length, $l\mu$, in order to avoid shifts in the SGV centroid as a result of absorption. For pure cobalt with the use of thermal neutrons (*25 meV*), $l\mu$ is *2.57 mm* (Ref. [38]).

Table 3. Scattering properties of ASTM F75 in comparison with Fe at a wavelength of 1.8 Å.

Property	**ASTM F75** (Ref. [82, 87])	**Iron** (Ref. [82, 87])
Avg. coherent scattering length (cm)	0.33×10^{-12}	0.95×10^{-12}
Coherent cross section (cm^2)	1.37×10^{-24}	11.2×10^{-24}
Incoherent cross section (cm^2)	2.19×10^{-24}	0.4×10^{-24}
Absorption cross section (cm^2)	23.56×10^{-24}	2.6×10^{-24}

4.2.3 Strain-release techniques

4.2.3.1 Centre-hole drilling

The centre-hole drilling technique involves inducing a hole into the centre of a specialised strain gauge rosette, see Figure 8. As the material is removed, residual stress is relieved and equilibrium is obtained by the displacement of material, which is measured by the strain gauges. The measured strains are then utilised to back-calculate residual stress magnitudes. The method is standardised[65] and there exists an excellent good-practice guide[88] and a technical note[89].

As outlined in the section 4.2.1 the technique can only be applied to the bone-cut surfaces of a femoral and due to drill access restrictions, at most 2-measurements per femoral can be made, as indicated in Figure 1. For thick components (i.e. those with a thickness of 1.2 D, where D is the diameter of the gauge circle, see Figure 8), stress up to 80 % of the materials' yield strength can be determined[65, 89]. The centre-hole drilling technique can be applied incrementally, to determine a stress gradient up to a depth of 50% of the hole diameter[88]. Vishay's largest strain-gauge rosette, which is required to mitigate potential anisotropic effects (see section 4.2.3.1.1), allows for a *2 mm* depth capability. This is significant considering the thickest section of a typical femoral is approximately *8 mm*.

Section 4.2.3.1.3 outlines centre-hole drilling measurements carried out by Veqter Ltd, Unit 8 Unicorn Business Park, Whitby Road, Brislington, Bristol, BS4 4EX, UK. However, ASTM F75 femoral castings pose a number of challenges for the technique as outlined in sections 4.2.3.1.1 and 4.2.3.1.2.

4.2.3.1.1 Grain-size

The centre-hole drilling method assumes isotropic material properties[65], however as outlined in section 4.2.1, the gauge volume may become anisotropic. Ref. [90] states that a number of publications exist which show that the influence of material texture can be neglected. However, the authors have not yet identified these publications.

Effects of elastic anisotropy are expected to be reduced for residual stress determination methods which contain a large number of grains within their gauge volumes. Therefore Vishay's largest strain gauge rosette, EA-06-125RE-120, is required. Based on a recommendation that the gauge length be at least 5 times the grain diameter[91] EA-06-

125RE-120 can be applied to a material with grain diameters up to *636 μm*, which is comparable to the grain sizes observed in this study (Figure 3). However use of this gauge will not fulfil recommended location requirements (see Table *4*). Calibration coefficients to account for significant departures from the ideal application could be determined by the use of finite-element modelling[88], as carried out by Ref [92].

Table 4. Vishay strain-gauge rosette dimensions[93] and corresponding required sample dimensions as outlined in Ref. [65]. See Figure 8 for a graphical description of each dimension.

Vishay gauge #	Gauge length, L (mm)	Grid centre-line diameter, D (mm)	Typical hole diameters, d (mm)	Min. sample thickness, t (mm)	Min. distance from gauge centre point to edge/boundary, y (mm)
EA-06-31RE-120	0.79	2.56	0.8 - 1	2.56	3.84
EA-06-62RE-120	1.57	5.13	1.5 - 2	5.13	7.695
EA-06-125RE-120	3.18	10.26	3 - 4.1	10.26	15.4
Femoral dimensions				Thickness: varies (see Figure 1), max of ≈8 mm	≈10 mm

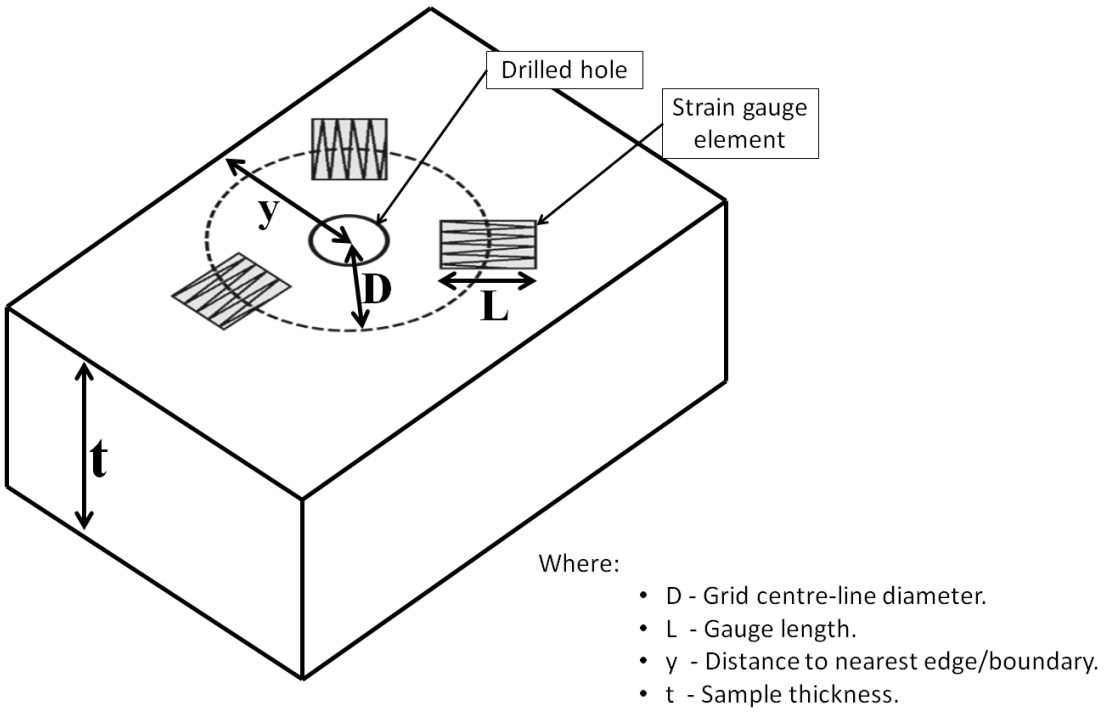

Figure 8. Schematic of centre-hole drilling arrangement.

4.2.3.1.2 Drilling method

The manner in which the hole is induced and deviations in the geometry of the hole can influence measured strains[94-97]. The most common method of inducing the hole is by the use of a high-speed air-turbine[65], but a number of alternative drilling techniques also exist[65, 88, 97, 98]. ASTM F75 is a difficult material to machine, as outlined in section 3.3, therefore problems such as sticking of cutting tools, poor geometry of cut surfaces and dulling of cutting tools may arise with mechanical drilling methods.

Ref. [97] determined that high-speed drilling applied to stress-free Stellite 100 (composition given in Appendix A) could result in significant error magnitudes due to induced stress. No details of the stress-relieving heat-treatment applied by Ref. [97] are given. Should Stellite 100, a cobalt alloy, have broadly similar high-temperature material properties to ASTM F75, then it may have been possible for residual stress magnitudes in the region of those observed by Ref. [97], to remain (see Table 5). However, should the errors observed by Ref. 95 be a result of the drilling technique, their influence will diminish for higher stress magnitudes where the strain response of the material would be larger.

Ref. [94] investigated the influence of various hole drilling parameters on the accuracy of the centre-hole drilling technique. In contrast to Ref. [97], Ref. [94] concluded that errors were related to hole imperfections and were not the result of induced stress. However, it should be considered that the machinability ratings of ASTM F75 and likely Stellite 100, utilised by Ref. [97], are considerably lower than that of the 6061-T651 aluminium or 304 stainless steel utilised by Ref. [94], see Figure 4.

It is anticipated on the basis of findings of both Ref. [97] and [94] that provided a straight-sided flat-bottomed hole is achieved; high-speed drilling will at-least be suitable for application to cast ASTM F75 femoral where large magnitudes of residual stress are expected.

Table 5. JMatPro©[47] predicted material properties for ASTM F75.

Solidus	1230 °C
Yield stress at 1220 °C (0.001 strain rate)	107 MPa
Yield stress at 1220 °C (10^{-6} strain rate)	34 MPa

4.2.3.1.3 Centre-hole drilling feasibility measurements

Veqter Ltd. carried out the incremental centre-hole drilling measurements on two femorals as part of this work, one in the as-cast condition (ICHD 1) and one which experienced surface-induced plastic deformation (ICHD 2). Sample ICHD 2 experienced the same manufacturing process[‡] as the sample used for X-ray measurement XRD 2. Neither sample was cast with an inoculant (see section 3.1.2). Veqter utilised a *1.6 mm* inverted-cone dental-carbide-bur with an orbital drilling method and *~10,000 RPM* spindle speed in order to successfully drill a *4 mm* diameter hole in the centre of a Vishay EA-06-125RE-120 strain gauge. Note ASTM E837 requirements for sample thickness and distance of the gauge from boundaries were not fulfilled (see Table 4).

4.2.3.1.3.1 Results and discussion

The hoop-stress results are shown in Figure 9 with the use of two types of calibration constants, those outlined in Ref. [65] and those determined by Veqter Ltd. for intermediate thickness components[92]. Additionally, averaged X-ray results for measurement XRD 2, reported in section 4.2.2.2.3 are included. Cross-sections of the drilled holes were inspected and found to be straight-sided and flat bottomed, with some rounding at the hole's bottom-to-side intersection.

Figure 9 indicates a noticeable change in the near-surface residual stress between ICHD 1 and ICHD 2. The induced compressive layer extends approximately 0.7 mm deep into the component, which can be considered significant as this component was approximately *8 mm* thick at its thickest section. The X-ray diffraction results compliment the centre-hole drilling results as they suggest the compressive stress profile would continue to increase towards the surface. It is expected that a balancing tensile stress exists deeper within the component.

The centre-hole drilling is a feasible technique as it was capable of distinguishing between two significantly different stress states. Additionally it was anticipated that the manufacturing process applied to ICHD2 would induce a near-surface compressive layer of stress of significant magnitudes, which is also supported by the X-ray diffraction results.

[‡] Specific details of manufacturing process cannot be published due to intellectual property restrictions.

However the degree of influence of stress induced from drilling and the effect of the materials coarse grain structure are unknown.

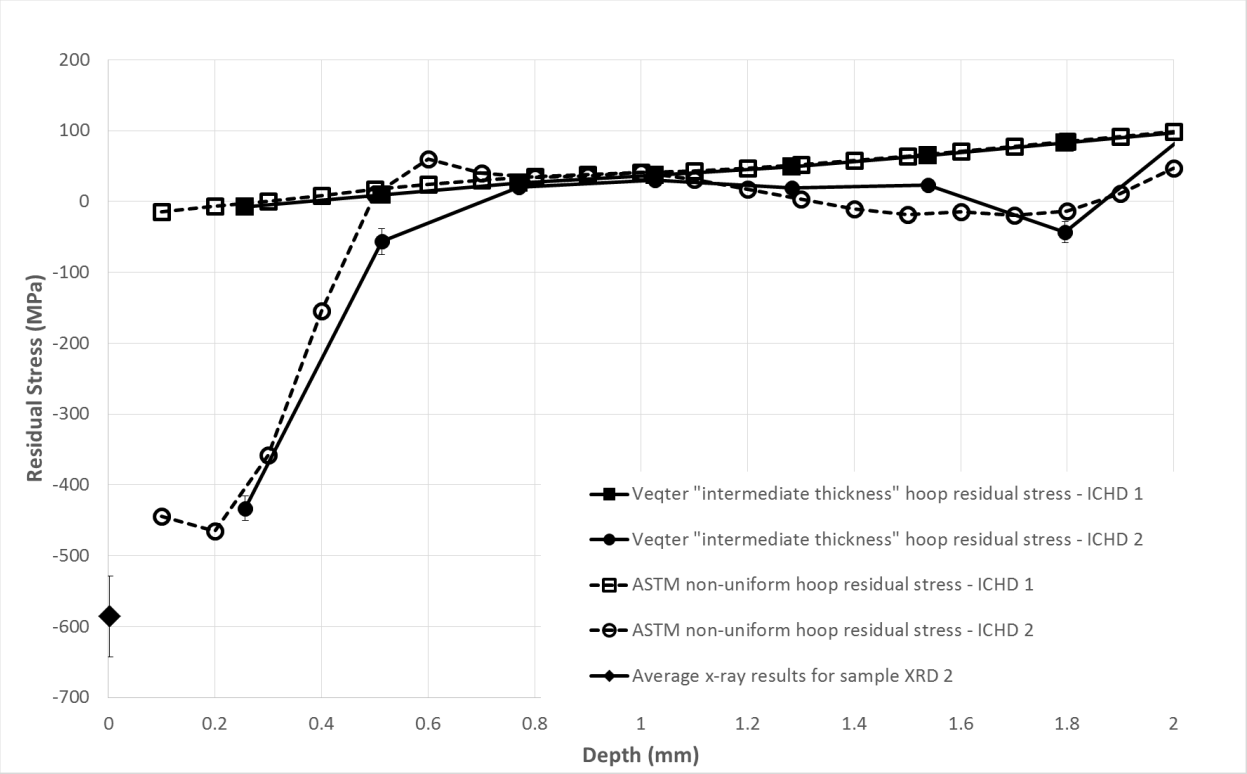

Figure 9. Centre-hole drilling residual stress results in the hoop-direction for an as-cast femoral (ICHD 1) and a femoral which experienced surface induced plastic deformation (ICHD 2). Elastic modulus: 220 GPa (based on an average of elastic modulus observed by Ref. 24) Poisson's ratio: 0.33. Averaged results for X-ray measurement XRD 2, which was carried out on a sample which experienced the same manufacturing process as ICHD 2, are also included. Note: The sample utilised for measurement XRD 2 was not the same component utilised for ICHD 2.

4.2.3.2 Contour method

The contour method involves sectioning a component utilising a wire-EDM and measuring the resultant cut-surface profile, which is dictated by the released residual stress[99]. As a result, 2-D spatial variation of the residual stress normal to the cut-surface is obtained. A number of excellent publications exist which detail the contour method and its application[99-102]. Additionally, the Los Alamos National Laboratory maintain a useful website dedicated to the contour method which includes an extensive record of relevant literature[103].

The theory of the contour method is based on Bueckner's superposition principal and is illustrated in Figure 10. Step A in Figure 10 shows the component within which stress is to be determined. Step B shows the sectioned part which has deformed as a result of the relieved residual stress. Step C shows a situation where the free surface of B has been forced back to its original shape from step A. The original stress state in A is equal to the stress state in B plus the change in stress from step C. As the stress state for step B is not known, the original stress state in A cannot be determined. However stress normal to the free-surface of B must be zero, therefore step C will give stresses along the plane of that cut, which is the principle of the contour method. Step C, which is achieved by finite element modelling, will also determine the change in stress, as a result of the cut, throughout the part. [99]

4.2.3.2.1 Requirements and limitations

Provided suitable cutting parameters are selected, wire-EDM can be utilised to section conductive components with little influence to bulk residual stress magnitudes[104, 105]. The wire-EDM cutting parameters will dictate the surface roughness of the cut plane, which subsequently influences the minimum possible spatial resolution of the contour method, therefore suitable wire-EDM cutting parameters need to be determined[100, 102]. However, the contour method is not suitable for the determination of near-surface residual stress unless special precautions are taken[106, 107].

The contour method is not limited by the size of the component, but by the magnitude of distortion on the contour surface. A minimum peak-valley surface contour of 10-20 µm is recommended[100]. The method is well suited to large components, as contours tend to be

more easily measured in comparison to smaller components, but has been applied successfully to components 2-6 mm thick[100], which is comparable with the thickness of femoral castings.

In order to prevent movement of the sample as a result of redistributed residual stress during sectioning, which will influence the surface contours, careful clamping of the sample either side of the cut-plane is required[99, 100, 102]. Complex shapes, such as the femoral, require suitable clamping solutions. Custom fixtures may be required.

4.2.3.2.2 Elastic modulus

The contour method does not necessarily require the assumption of homogenous elastic modulus as elastic anisotropy can be accounted for in finite element models, if the spatial distribution of the elastic modulus throughout the part is known[100, 108]. It is required that the part to which the contour method is applied has symmetrical stiffness either side of the cut plane, the size of which can be estimated as a distance from the cut surface of 1.5 times the part thickness[100]. This requirement limits the locations at which the method could be applied on the complex-shaped femoral component. Finite element analysis can be utilised to estimate errors in the case of asymmetric components, errors tend to be small unless the degree of asymmetry is high[100].

Considering the potential for significant elastic anisotropy, highlighted in section 3.2, it is a concern that assuming isotropic elastic modulus could influence the contour method results. However, of all the strain-release techniques, the contour method will include the contribution from largest number of grains. Grains across the entire contour-cut surface and to some depth behind the cut-surface, will contribute to the elastic modulus of the gauge area[109]. However, should the part be textured as a result of the solidification process (see section 3.2), then elastic modulus may vary between each contour-cut plane on the same part.

An ideal scenario would be application of energy-selective neutron transmission tomography to determine the grain structure and orientation of the component in the vicinity of the applied contour method cut [110-112]. A finite element model could then be developed with directionally dependent elastic modulus applied to each grain. Such a model would replicate the true elastic modulus properties of the component.

4.2.3.2.3 Feasibility study overview

In collaboration with Stress Map at the Open University, Walton Hall, Milton Keynes, MK7 6AA, UK, a feasibility study was carried out on the application of the contour method to ASTM F75 femoral castings. The method was applied to parts with the same processing history as ICHD 1 and ICHD 2 from section 4.2.3.1.3, which shall be referred to as CM1 and CM2 respectively. Two cuts per femoral were applied with one cut returning data in the axial direction and the other cut returning data in the hoop direction (see Figure 11).

Isotropic material properties, as given for the centre-hole drilling method (see Figure 9), were assumed for the application of the contour method. From initial inspection of results from CM2, the sign, location and magnitude of stresses determined appeared feasible and displacement data did not show any unusual variations. The expected residual stress state for sample CM2, which experienced surface induced plastic deformation, was a large magnitude exterior compressive stress region with a balancing tensile interior region. Contour method results from CM2 exhibited this compressive exterior layer, also identified in section 4.2.3.1.3, and also revealed the balancing tensile interior region. Magnitudes of stress observed for sample CM2 were significantly larger than those for CM1, which is in agreement with observations from the centre-hole drilling measurements. A more detailed publication of the application of the contour method and the results obtained will follow. However, the contour method is anticipated to be the most promising residual stress determination technique for application to ASTM F75 castings as for the following reasons:

- 2-D spatial variation of residual stress can be assessed in the direction of interest, i.e. hoop direction of the femoral.
- Use of wire-EDM eliminates concerns of inducing residual stress during sectioning, thus mitigating the difficult machining properties of the material.
- The gauge-area will include a large number of grains, which will help reduce the influence of elastic anisotropy.
- Elastic anisotropy, if deemed problematic, could be catered for in finite element computer models.

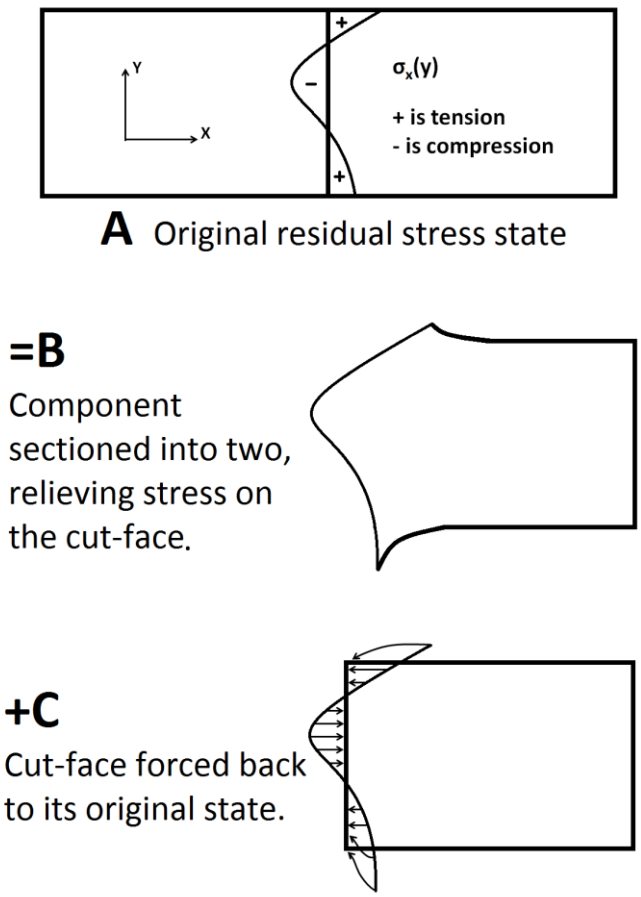

Figure 10. Superposition principle to determine residual stresses normal to the cut-surface of the contour method. Figure reproduced from Ref.[99].

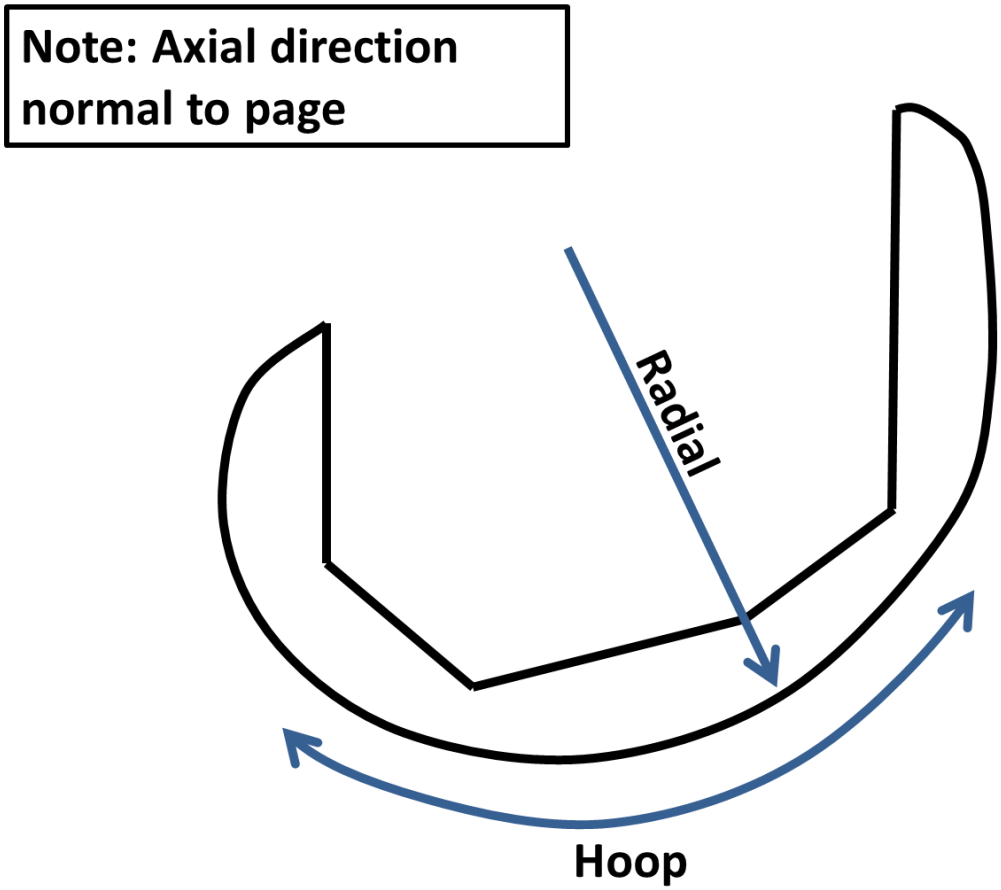

Figure 11. Cross-section view of a femoral with labelling of directional axes.

5 Summary

Residual stress inducement and/or redistribution has been identified as the source of ASTM F75 femoral distortion. Residual stress in ASTM F75 can result from non-uniform plastic deformation or a stress induced FCC-HCP phase transformation. A number of manufacturing processes have the ability to influence the residual stress state of the ASTM F75 femoral components; however a reliable residual stress determination technique is required to investigate the influence of each. Additionally it has been identified that the ASTM F75 femoral implants are likely elastically anisotropic on a macroscopic scale, which will have an influence on the magnitude of femoral distortion if a part-part variation in elastic modulus properties exists.

Each residual stress determination method has limitations associated with application to as-cast ASTM F75 femorals. A table in Appendix B compares all techniques covered in this article using a number of different comparison criteria. X-Ray diffraction has been identified a feasible method for determining surface residual stress of ASTM F75 femorals which have experienced plastic deformation on their surfaces, which results in refined diffracting domains. The method could be combined with layer removal techniques to obtain depth profiles; however the depth to which suitably refined grains exist is unknown and would depend on the severity of the plastic deformation.

The feasibility of neutron diffraction has yet to be definitively determined; experimentation is ongoing and a future publication will address this matter. However, as-cast ASTM F75 femorals are a challenging application for neutron diffraction due to their coarse grain structure and the difficult nuclear material properties of cobalt. Given the limited availability of neutron facility access and the long count times required to achieve adequate diffraction-peak-intensities, this method is not feasible for regular application.

The centre-hole drilling method is a feasible technique to determine large magnitude residual stress states, as potential errors from drilling-induced residual stress will diminish. ASTM F75 is a difficult material to drill, however use of suitable drilling burrs and drilling parameters can yield adequate drilled-hole quality, as achieved by Veqter Ltd. A straight-sided, flat bottomed hole is required to minimise errors. The residual stress distributions determined for the as-cast femoral show low magnitude residual stress and results for the

femoral which experience surface induced plastic deformation showed large magnitude, near surface, compressive stress. Unknown influence on the results was the potential of elastic anisotropy and induced stress from the drilling method.

The contour method is the most promising technique of all those reviewed as it has the ability to address all limitations identified; wire-EDM alleviates the potential to induce stress during cutting and elastic anisotropy could be incorporated into finite element models should the grain structure and orientations be determined. Additionally the method can return 2-D spatial variation of residual stress normal to the cut-plane, which can be applied to determine residual stress in the directions of interest within the femoral.

On a qualitative basis, all results reported are in agreement. The femorals which experienced surface induced plastic deformation would have been anticipated to have a compressive exterior layer of residual stress with a balancing tensile interior region. The magnitude of this stress state within these femorals was anticipated to be larger than those of the as-cast femoral. These anticipated stress states were identified using the centre-hole drilling method and from initial inspection of the contour method results. Additionally, x-ray diffraction revealed that a large compressive stress exists on the surface of the femoral which experienced surface induced plastic deformation, which suggests the compressive exterior region, identified by the centre hole drilling method and the contour method, continues towards the surface.

6 Conclusions

- Residual stress is the source of ASTM F75 femoral distortion and is the result of in-homogenous plastic deformation and/or a strain-induced FCC-HCP phase change.
- The following residual stress determination methods are not suitable for application to cast ASTM F75 femorals: magnetic methods, ultrasonic methods, layer removal methods, sectioning, the slitting method, deep-hole drilling and ring coring.
- X-ray diffraction is a feasible residual stress determination method for cast ASTM F75 components which have experienced plastic deformation on their surface.
- Centre-hole drilling is a feasible technique; however the degree of influence of stress induced from drilling and the effect of the materials' coarse grain structure are currently unknown.
- As-cast ASTM F75 components are a challenging application for neutron diffraction due their coarse grain structure and the difficult nuclear material properties of cobalt.
- A proprietary manufacturing process which induces plastic deformation on the surface of ASTM F75 femorals has the potential to significantly influence their bulk residual stress state, as determined by centre-hole drilling and unpublished contour method results. This stress will influence femoral distortion following material removal.
- The contour method is the most promising residual stress determination technique for application to cast ASTM F75 femorals.

7 Acknowledgements

The authors would like to acknowledge the following sources of funding:

- Irish Research Council, award number EPSPG/2012/357.
- DePuy (Ireland)
- MedCast, a Marie Curie FP7 funded project (Project reference number: 251269).
- Experiments at the ISIS Pulsed Neutron and Muon Source were supported by a beam time allocation and travel expense funding from the Science and Technology Facilities Council.
- Experiments at the Helmholtz-Zentrum-Berlin were supported by funding received from the European Union's Seventh Framework Programme for research, technological development and demonstration under the NMI3-II Grant number 283883.

The authors would also like to acknowledge the following personnel, universities and companies for conducting residual stress determination measurements and/or providing technical consultation:

- Dr. Mike Woodard and Mr. Yoshi Teramoto at Pulstec Industrial Co. Ltd., 7000-35, Nakagawa, Hosoe-cho, Kita-ku, Hamamatsu-City, Shizuoka Pref., 431-1304, Japan.
- Dr. Andrew Winn at the University of Manchester, Grosvenor Street, Manchester, M1 7HS, UK.
- Dr. Robert Wimpory at Helmholtz-Zentrum-Berlin, Hahn-Meitner-Platz 1, 14109 Berlin, Germany.
- Dr. Joe Kelleher at ISIS, Science and Technology Facilities Council, Rutherford Appleton Laboratory, Harwell Oxford, Didcot, OX11 0QX, UK.
- Dr. Xavier Ficquet and Dr. Ed Kingston at Veqter Ltd., Unit 8 Unicorn Business Park, Whitby Road, Brislington, Bristol, BS4 4EX, UK.
- Dr. Sanjooram Paddea and Dr. Yelí Traoré at the Open University, Walton Hall, Milton Keynes, MK7 6AA, UK.
- Mr. Anton Chittey, Vishay Measurements Group UK Ltd., Stroudley Road, Basingstoke, Hampshire, RG24 8FW, UK.
- Dr. Mike Prime, Los Alamos National Laboratory, Los Alamos, NM 87545, USA.

8 Appendix A – Material composition comparison

Element	Composition (%, mass/mass)			
	ASTM F75 (Ref. [5])		Stellite #21 (Ref. [113])	Stellite #100 (Ref. [113])
	min	max		
Chromium	27.00	30.00	27	34
Molybdenum	5.00	7.00	5.5	-
Nickel	-	0.50	2.5	3 (max)
Iron	-	0.75	3 (max)	1 (max)
Carbon	-	0.35	.25	2
Silicon	-	1.00	1.5	1
Manganese	-	1.00	1	1
Tungsten	-	0.20	-	19
Phosphorous	-	0.020	-	-
Sulphur	-	0.010	-	-
Nitrogen	-	0.25	-	-
Aluminium	-	0.10	-	-
Titanium	-	0.10	-	-
Boron	-	0.010	-	-
Cobalt	balance	balance	balance	balance

9 Appendix B – Residual stress determination comparison table

Comparison criteria	Influence of criteria on residual stress determination method for CoCrMo castings			
	X-ray diffraction	**Neutron diffraction**	**Centre-hole drilling**	**Contour method**
Coarse grain-size	Evident as poor diffraction spectrums result on as-cast surfaces. Method is applicable to surfaces which have been plastically deformed.	Evident as the number of peaks in ToF diffraction spectrums can vary depending on the location of the measurement.	N/A	N/A
Elastic anisotropy	Cannot influence this method. A refined grain structure is required to obtain a suitable diffraction peak. Additionally, diffraction-plane specific elastic properties are utilised.	Unknown. The use of bulk material properties of elastic modulus following the fitting of ToF diffraction spectrums may be an inadequate assumption considering the potential for macroscopic elastic anisotropy.	Unknown. Large grains may result in a variation in elastic modulus seen by each strain gauge element.	Unknown. Spatial variations in elastic modulus normal to the cut-plane could potentially exist.
Spatial resolution	Typically a 2 mm diameter aperture.	Limited by grain size. Typically a 2x2x2 mm^3 gauge volume. Available gauge volume sizes can vary from instrument to instrument and on the expected stress gradient.	Stresses are averaged over 4 mm diameter hole with 0.2 mm depth increments.	Dependent on surface roughness of the wire-EDM cut.
Depth capability	≈5 µm. Method could be combined with layer removal techniques.	Total path length in CoCrMo limited to approximately 5 mm.	2 mm maximum from the surface of the component.	Limited by the magnitude of the cut-surface profile and the ability to section the component in a suitable manner. A minimum peak-valley surface contour of 10-20 µm is recommended.
Induced stresses during measurement	N/A	N/A	Potential influence from the drilling technique and surface preparation for strain gauge application.	Negligible provided suitable wire-EDM cutting parameters are used.
Geometry	Limited to flat surfaces or gentle curves.	Limited by paths lengths.	This method requires flat surfaces. ASTM standard outlines requirements for component thickness and distance of the drilled hole from boundaries.	-Geometric symmetry about the cut plane is required. -Clamping of complex shapes may require custom solutions.
Other material properties	Requires use of manganese x-ray tube to avoid fluorescence.	Difficult neutron scattering properties due to large absorption and incoherent scattering cross-sections.	-High elastic modulus results in small strain responses. -Rapid work hardening and high ultimate tensile strength make the material difficult to drill.	High elastic modulus results in smaller magnitude cut-surface contours.

10 References

1. OECD: 'Hip and knee replacement', in 'Health at a Glance 2013: OECD Indicators', 2013, Paris, OECD Publishing.
2. US Census Bureau, *US and world population clock (31 Dec 2011)*. 2015: http://www.census.gov/popclock/ [accessed 16 Apr 2015].
3. S. Kurtz, K. Ong, E. Lau, F. Mowat, and M. Halpern, *The J. of Bone and Jt. Surg.*, 2007, **89**, 780-785.
4. J. A. Disegi, R. L. Kennedy, and R. Pillar, eds. *ASTM STP 1365: Cobalt-based alloys for biomedical applications*, 1999, USA, ASTM International.
5. ASTM, *ASTM F75: Standard specification for cobalt - 28 chromium-6 molybdenum alloy casting and casting ally for surgical implants*. 2012, ASTM International: USA.
6. M. Niinomi, T. Hanawa, and T. Narushima, *JOM*, 2005, **57**(4), 18-24.
7. ASM International: 'Casting', in 'ASM Handbook', 1992, USA, ASM International.
8. ASTM, *ASTM F2083: Standard specification for knee replacement prosthesis*. 2012, ASTM International: USA.
9. M. B. Prime and M. L. Steinzig, *Adv. Mat. Res.*, 2014, **996**, 234-242.
10. P. J. Withers and H. K. D. H. Bhadeshia, *Mat. Sci. and Tech.*, 2001, **17**(4), 355-365.
11. F. A. Kandil, J. D. Lord, A. T. Fry, and G. P. V: 'A review of residual stress measurement methods - a guide to technique selection'; 2001, UK, NPL.
12. P. J. Withers, *C. R. Physique*, 2007, **8**, 806-820.
13. N. D. Rossini, M. Dassisti, K. Y. Benyounis, and A. G. Olabi, *Mat. and Des.*, 2012, **35**, 572-588.
14. R. G. Treuting, H. B. Wishart, J. J. Lynch, and D. G. Richards: 'Residual stress measurements'; 1952, Ohio, ASM.
15. P. J. Withers and H. K. D. H. Bhadeshia, *Mat. Sci. and Tech.*, 2001, **17**(4), 366-375.
16. G. S. Schajer and C. O. Ruud: 'Overview of residual stresses and their measurement', in 'Practical residual stress measurement methods', (ed. G. S. Schajer), 1-27; 2013, UK, John Wiley and Sons.
17. S. Cai, M. R. Daymond, and Y. Ren, *Mat. Sci. and Eng. A*, 2013, **580**, 209-216.
18. M. L. Benson, P. K. Liaw, H. Choo, D. W. Brown, M. R. Daymond, and D. L. Klarsrom, *Mat. Sci. and Eng. A*, 2011, **528**(18), 6051-6058.
19. P. Huang and H. F. López, *Mat. Lett.*, 1999, **39**, 244-248.
20. A. Salinas-Rodrígeuz: 'The role of FCC-HCP phase transformation during the plastic deformation of Co-Cr-Mo-C alloys for biomedical applications', in 'ASTM STP 1365: Cobalt-base alloys for biomedical applications', (eds. J. A. Disegi, et al.), 108-110; 1999, USA, ASTM International.
21. H. K. D. H. Bhadeshia: 'Worked examples in the geometry of crystals'; 1987, UK, The Institute of Metals.
22. R. Kaiser: 'Study of the effect of casting variables and heat treatment procedures on the microstructure and mechanical properties of Co-Cr-Mo biomedical alloy', PhD thesis, University College Dublin, 2013.
23. R. Kaiser, K. Williamson, C. O'Brien, and D. J. Browne, *Metall. and Mat. Trans. A*, 2013, **44**(12), 5333-5342.
24. R. Kaiser, K. Williamson, C. O'Brien, S. Ramirez-Garcia, and D. J. Browne, *J. of the Mech. Behav. of Biomed. Mat.* , 2013, **24**, 53-63.
25. H. F. López and A. J. Saldivar-Garcia, *Metall. and Mat. Trans. A*, 2008, **39**(1), 8-18.
26. J. R. Davis: 'Phase diagrams of binary and ternary cobalt systems', in 'ASM speciality handbook: nickel, cobalt and their alloys', 356-361; 2000, USA, ASM International.
27. C. Montero-Ocamp, R. Juarez, and A. Salinas-Rodrígeuz, *Metall. and Mat. Trans. A*, 2002, **33**(7), 2229-2235.
28. C. D. Opris, R. Liu, M. X. Yao, and X. J. Wu, *Mat. and Des.*, 2007, **28**(2), 53-61.

29. J. V. Giacchi, C. N. Morando, O. Fornaro, and H. A. Palacio, *Mat. Charac.*, 2011, **62**(1), 53-61.
30. Y. Bedolla-Gill, A. Juarez-Hernandez, A. Perez-Unzueta, E. Garcia-Sanchez, R. Mercado-Solis, and M. A. L. Hernandez-Redriguez, *Revista Mexicana De Física*, 2009, **55**(1), 1-5.
31. Alfirano, S. Mineta, S. Namba, T. Yoneda, K. Ueda, and T. Narushima, *Metall. and Mat. Trans. A*, 2011, **42**(7), 1941-1949.
32. R. Kaiser, D. J. Browne, and K. Williamson: 'Investigation of the effects of cooling rate on the microstructure of investment cast biomedical grade Co alloys', The 3rd International Conference on Advances in Solidification Processes, Aachen, 2011, IOP Science.
33. M. Gomez, H. Mancha, A. Salinas, J. L. Rodríguez, J. Escobedo, M. Castro, and M. Mendez, *J. of Biomed. Mat. Res.*, 1997, **34**(2), 157-163.
34. Y. Liao, R. Pourzal, P. Stemmer, M. A. Wimmer, J. J. Jacobs, A. Fischer, and L. D. Marks, *J. of the Mech. Behav. of Biomed.*, 2012, **12**, 39-49.
35. H. Ghazvinizadeh, M. Meratian, A. Kermanpur, M. H. Fathi, and H. Minouei, *Int. J. of Eng.*, 2011, **24**(1), 49-53.
36. K. Harris and S. Sikkenga: 'Investment cast cobalt alloys', 24th BICTA conference on investment casting, Oxford, 1999.
37. P. R. Beeley: 'Foundry technology'; 1980, London, Butterworths.
38. M. T. Hutchings, P. J. Withers, M. Holden, and T. Lorenzten: 'Introduction to the characterization of residual stress by neutron diffraction'; 2005, USA, CRC Press.
39. E. J. Carozza, L. Burd, and E. R. Miller: 'Anisotropic surgical prosthesis (EP 0145617A2)', Patent, 1984.
40. M. J. Pappas and F. Buechel: 'Prosthetic device with predetermined crystal orientation (EP 0163920A2)', Patent, 1985.
41. D. M. Stefanescu: 'Science and engineering of casting solidification'; 2009, USA, Springer.
42. A. Kelly and K. M. Knowles: 'Crystallography and crystal defects'; 2012, UK, John Wiley and Sons.
43. G. E. Dieter: 'Mechanical Metallurgy'; 1988, UK, McGraw-Hill.
44. J. Gump, H. Xia, M. Chirita, R. Sooryakumar, M. A. Tomaz, and R. Harp, *J. of Appl. Phys.*, 1999, **86**(11), 6005-6009.
45. Metal Suppliers Online. '430 F stainless steel material property data sheet [online], available: http://www.suppliersonline.com/propertypages/430F.asp', 2016 [viewed 29 March 2016].
46. K. Rajan and J. B. Vander Sandea, *J. of Mat. Sci.*, 1982, **17**, 769-778.
47. Sente Software Ltd., *JMatPro*. 2014: UK.
48. T. J. Drozda and C. Wick, eds. *Tool and manufacturing engineers handbook - Volume I: Machining*, 1983, USA, SME.
49. G. S. Schajer, ed. *Practical residual stress measurement methods*, 2013, UK, John Wiley and Sons.
50. G. Totten, M. Howes, and T. Inoue: 'Handbook of residual stress and deformation of steel'; 2002, USA, ASM International.
51. J. Lu, ed. *Handbook of measurement of residual stresses*, 1996, USA, The Fairmount Press.
52. J. F. Flavenot: 'Layer removal method', in 'Handbook of measurement of residual stress', (ed. J. Lu), 35-48; 1996, USA, The Fairmount Press.
53. Y. Ueda: 'Sectioning methods', in 'Handbook of measurement of residual stress', (ed. J. Lu), 35-48; 1996, USA, The Fairmount Press.
54. E. Procter and E. M. Beaney: 'The trepan or ring core method, centre-hole method, Sach's method, blind hole methods, deep hole technique', in 'Advances in surface treatments; technology-application-effects', (ed. A. Nikul-Lari), 165-199; 1987, UK, Permagon Press.
55. D. J. Buttel: 'Magnetic methods', in 'Practical residual stress measurement methods', (ed. G. Schajer), 225-258; 2013, UK, John Wiley and Sons Ltd.

56. R. B. Thompson, W. Y. Lu, and A. V. Clark: 'Ultrasonic methods', in 'Handbook of measurement of residual stresses', (ed. J. Lu), 1996, USA, The Fairmount Press.
57. S. Kiel, *Exp. Tech.*, 1992, **16**(5), 17-24.
58. K. P. Milbrandt, *Proc SESA*, 1951, **9**(1), 63-74.
59. G. S. Schajer and G. Ray: 'Hole-drilling and ring core methods ', in 'Handbook of measurement of residual stresses', (ed. J. Lu), 1996, USA, The Fairmount Press.
60. HBM, *Strain gauge catalogue*. n.d.: http://www.hbm.com/en/menu/products/strain-gauges/strain-gauge-catalog/ [accessed 27 Aug 2015].
61. M. R. Hill: 'The slitting method', in 'Practical residual stress measurement', (ed. G. S. Schajer), 89-108; 2013, UK, John Wiley and Sons.
62. W. Cheng and I. Finnie, *Residual stress measurement and the slitting method*. 2007, Springer: USA.
63. D. J. Smith: 'Deep hole drilling', in 'Practical residual stress measurements', (ed. G. S. Schajer), 2013, UK, John Wiley and Sons.
64. D. M. Stefanescu, C. E. Truman, and D. J. Smith, *The J. of Strain Anal. for Eng. Des.*, 2004, **39**(5), 483-497.
65. ASTM, *ASTM E837: Standard method for determining residual stresses by the hole drilling strain gauge method*. 2013, ASTM International: USA.
66. R. Paynter, A. H. Mahmoudi, M. J. Pavier, D. A. Hills, D. Nowell, C. E. Truman, and D. J. Smith, *The J. of Strain Anal. for Eng. Des.*, 2008, **44**(1), 45-54.
67. P. Prevéy: 'X-ray diffraction residual stress techniques', in 'Metals Handbook', (ed. K. Mills), 9 edn, 1986, USA, ASM.
68. V. Hauk: 'Structural and residual stress analysis by nondestructive methods'; 1997 The Netherlands, Elsevier.
69. A. C. Vermeulen: 'An elastic constants database and XEC calculator for use in XRD residual stress analysis*',* Denver X-Ray Conference, Colorado, 2001, ICDD.
70. ISO, *ISO/TS 21432: Non-destructive testing - standard test method for determining residual stresses by neutron diffraction* 2005, ISO: Geneva.
71. BSI, *BS EN 15305: Non-destructive testing. Test method for residual stress analysis by X-ray diffraction*. 2008, BSI: London.
72. B. D. Cullity and S. R. Stock: 'Elements of X-ray diffraction'; 2001, New Jersey, Prentice Hall.
73. C. Kittel: 'Introduction to solid state physics'; 1996, New York, John Wiley and Sons.
74. B. Eigenmann and E. Macherauch, *Materialwissenschaft und Werkstofftechnik*, 1996, **27**(9), 426-437.
75. M. E. Fitzpatrick, A. T. Fry, P. Holdway, F. A. Kandil, J. Shackleton, and L. Suominen: 'Determination of residual stresses by X-ray diffraction - Issue 2', in 'Measurement good practice guide Bo. 52', 2005, UK, NPL.
76. I. C. Noyan and J. B. Cohen: 'Residual stress measurement by diffraction and interpretation'; 1987, USA, Springer.
77. ASTM, *ASTM E112: Standard test methods for determining average grain size*. 2013, ASTM International: USA.
78. J. S. Robinson and W. Redington, *Mat. Charac.*, 2015, **105**, 47-55.
79. T. Sasaki and Y. Kobayashi: 'X-ray multiaxial stress analysis using two debye rings*',* Denver X-ray conference, Colorado, 2008, ICDD.
80. L. Pintschovius: 'Macrostresses, microstresses and stress tensors', in 'Measurement of residual and applied stress using neutron diffraction, Nato ASI Series', (eds. M. T. Hutchings, et al.), 1992, UK, Springer Science + Business Media.
81. ISO, *ISO/TTA 3: Polycrystalline materials - determination of residual stresses by neutron diffraction*. 2001, ISO: Geneva.
82. T. M. Holden: 'Neutron diffraction', in 'Practical residual stress measurement methods', (ed. G. S. Schajer), 195-223; 2013, UK, Wiley.

83. C. Ohms: 'Residual stresses in thick bi-metallic fusion welds: a neutron diffraction study', PhD thesis, Delft University of Technology, The Netherlands, 2013.
84. T. M. Holden, Y. Traore, J. James, J. Kelleher, and P. John Bouchard, *J. of Appl. Crys.*, 2015, **48**(2), 582-584.
85. C. Larsson, T. M. Holden, M. A. M. Bourke, M. Stout, J. Teague, and L. E. Lundgren, *Mat. Sci. and Eng. A*, 2005, **399**(1-5), 49-57.
86. J. R. Santisteban, M. R. Daymond, J. A. James, and L. Edwards, *App. Crystall.*, 2006, **39**, 812-825.
87. V. F. Sears, *Neutron News*, 1992, **3**(3), 26-37.
88. P. V. Grant, J. D. Lord, and P. S. Whitehead: 'Measurement of residual stresses by the incremental hole drilling technique', in 'Measurement good practice guide No. 53 - Issue 2', 2006, UK, NPL.
89. Vishay Precision Group: 'Measurement of residual stresses by the hole-drilling strain gauge method - Technical note TN-503', in 2010, http://www.vishaypg.com/docs/11053/tn503.pdf [accessed 07 July 2015].
90. R. Oettel: 'The determination of uncertainties in residual stress measurement (using the hole drilling technique) - Code of practice No. 15', in 'Manual of codes of practice for the determination of uncertainties in mechanical tests on metallic materials - Project No. SMT4-CR97-2165', 2000, NPL.
91. A. Chittey (Vishay): Personal communication, 2013.
92. Y. Serra, X. Ficquet, and E. J. Kingston, *Adv. Mat. Res.*, 2014, **996**, 301-306.
93. Vishay Precision Group: 'Special use sensors- residual stress strain gauges', in 2010, http://www.vishaypg.com/docs/11516/resstr.pdf [accessed 07 July 2015].
94. M. Steinzig, D. Upshaw, and J. Ratsy, *Exp. Mech,*, 2014, **54**(99), 1537-1543.
95. M. T. Flaman, *Exp. Mech,*, 1982, **22**(1), 26-29.
96. M. T. Flaman and J. A. Herring, *Exp. Tech.*, 1986, **10**(1), 34-35.
97. M. T. Flaman and J. A. Herring, *Exp. Tech.*, 1985, **9**, 30-32.
98. H. T. Lee, J. Mayer, F. C. Hsu, W. P. Rehbach, T. Wireich, A. Dimyati, and T. Y. Tai, *J. of Eng. Mat. and Tech.*, 2006, **128**(3), 468-475.
99. M. B. Prime, *J. of Eng. Mat. and Tech.*, 2001, **123**(2), 162-168.
100. M. B. Prime and A. T. DeWald: 'The contour method', in 'Practical residual stress measurement methods', (ed. G. S. Schajer), 109-138; 2013, UK, John Wiley and Sons.
101. G. Johnson: 'Residual stress measurements using the contour method', PhD thesis, University of Manchester, UK, 2008.
102. F. Hosseinzadeh, J. Kowal, and P. J. Bouchard, *The J. of Eng.*, 2014.
103. Anon. 'The contour method for measuring residual stress [online], available: http://www.lanl.gov/contour/', 2016 [viewed 30 March 2016].
104. J. P. Kruth and P. Bleys, *Int. J. of Elec. Mach.*, 2000, **51**(1), 23-28.
105. W. Cheng, I. Finnie, M. Gremaud, and M. B. Prime, *J. of Eng. Mat. and Tech.*, 1994, **116**(1).
106. M. B. Prime and A. L. Kastengren: 'The contour method cutting assumptions: error minimization and correction', Society for experimental mechanics annual conference, Indiana, USA, 7-10 June, 2011, Exp. and Appl. Mech., 233-250.
107. M. B. Toparli, M. E. Fitzpatrick, and S. Gungor, *Exp. Mech*, 2013, **53**, 1705-1718.
108. M. B. Prime, H. Swenson, M. A. Buechler, M. Steinzig, B. Clausen, and T. Sinseros, *J. of Press. Vess. Techn.*, 2013, **135**(4).
109. M. B. Prime: Personal communication, 2016.
110. L. Josie, A. Steuwar, and E. Lehmann, *Appl. Phys. A*, 2010, **99**(3), 515-522.
111. J. R. Santisteban, L. Edwards, and V. Stelmukh, *Physica B: Condensed Matter*, 2006, **385-386**(Part 1), 636-638.
112. M. Boin, A. Hilger, N. Kardjilov, S. Y. Zhang, E. C. Oliver, J. A. James, C. Randau, and R. C. Wimpory, *J. of App. Crystallography*, 2011, **44**, 1040-1046.

113. Stellite, *Alloy database*. n.d.: http://www.stellite.com/alloydatabase/nominal.asp?b=Cobalt [accessed 24 July 2015].